

See discussions, stats, and author profiles for this publication at: <https://www.researchgate.net/publication/51537293>

# Quantitative Surface-Enhanced Raman Scattering Ultradetection of Atomic Inorganic Ions: The Case of Chloride

ARTICLE in ACS NANO · AUGUST 2011

Impact Factor: 12.88 · DOI: 10.1021/nn2025176 · Source: PubMed

---

CITATIONS

38

---

READS

62

## 7 AUTHORS, INCLUDING:



Dionysia Tsoutsi

Universitat Rovira i Virgili

4 PUBLICATIONS 74 CITATIONS

[SEE PROFILE](#)



Jose Maria Montenegro

University of Malaga

33 PUBLICATIONS 827 CITATIONS

[SEE PROFILE](#)



Wolfgang J. Parak

Philipps University of Marburg

359 PUBLICATIONS 18,101 CITATIONS

[SEE PROFILE](#)



Ramón A Alvarez-Puebla

Catalan Institution for Research and Advanc...

141 PUBLICATIONS 5,099 CITATIONS

[SEE PROFILE](#)

# Quantitative Surface-Enhanced Raman Scattering Ultradetection of Atomic Inorganic Ions: The Case of Chloride

Dionysia Tsoutsi,<sup>†</sup> Jose Maria Montenegro,<sup>‡</sup> Fabian Dommershausen,<sup>§</sup> Ulrich Koert,<sup>§</sup> Luis M. Liz-Marzán,<sup>†</sup> Wolfgang J. Parak,<sup>‡</sup> and Ramon A. Alvarez-Puebla<sup>†,\*</sup>

<sup>†</sup>Departamento de Química Física, and Unidad Asociada CSIC, Universidade de Vigo, 36310, Vigo, Spain, and <sup>‡</sup>Fachbereich Physik and <sup>§</sup>Fachbereich Chemie, Philipps Universität Marburg, Marburg, Germany

Rapid, sensitive and accurate quantitative detection of inorganic atomic ions is central in environmental, analytical and bioanalytical sciences. Many analytical techniques such as ion chromatography,<sup>1</sup> atomic absorption (or emission) spectroscopy,<sup>2</sup> or ion-sensitive electrodes<sup>3</sup> offer quantitative detection down to the ppm–ppb ( $\mu\text{M}$ –nM) regimes. Notwithstanding, these techniques require extensive sample preparation, may be destructive (in the case of chromatography or atomic absorption or emission spectroscopy) and, in the case of electrochemical methods, since the transduction element is bulky, it does not allow for the interrogation of microsystems such as cells. Further, while sodium and potassium membrane electrodes express good linearity over a wide physiological concentration range, chloride membrane electrodes show non-Nernstian response<sup>4</sup> and suffer from a number of electrolyte interferences.<sup>5</sup> In contrast, surface-enhanced Raman scattering (SERS) spectroscopy<sup>6–8</sup> is a nondestructive ultrasensitive technique that allows for the unequivocal identification of analytes in a wide variety of matrices, with no (or very little) need for processing prior to the analysis. Additionally, the transduction element, that is, nanostructured gold or silver, can be of nanometer dimensions and can be used with biological samples.<sup>9</sup> SERS has therefore been extensively investigated as a convenient tool for diagnosis, biodetection, and environmental monitoring.<sup>10,11</sup> However, as a molecular spectroscopy technique, SERS cannot be used to detect/recognize atomic species directly. Thus, within the 30 years since the discovery of the SERS effect, little research has been carried out toward the analysis of inorganic species in general and inorganic atomic ions in particular. However, several reports have been recently published

**ABSTRACT** Surface-enhanced Raman scattering (SERS) spectroscopy can be used for the determination and quantification of biologically representative atomic ions. In this work, the detection and quantification of chloride is demonstrated by monitoring the vibrational changes occurring at a specific interface (a Cl-sensitive dye) supported on a silver-coated silica microbead. The engineered particles play a key role in the detection, as they offer a stable substrate to support the dye, with a dense collection of SERS hot spots. These results open a new avenue toward the generation of microsensors for fast ultradetection and quantification of relevant ions inside living organisms such as cells. Additionally, the use of discrete particles rather than rough films, or other conventional SERS supports, will also enable a safe remote interrogation of highly toxic sources in environmental problems or biological fluids.

**KEYWORDS:** chloride · SERS · plasmonic platforms · ultrasensitive detection · quantitative analysis · colloidal particles

using indirect methods based on monitoring a capping agent with a high SERS cross-section, which is directly adsorbed onto the plasmonic surface. This agent is required to undergo a recognizable change, usually geometrical or electronic, upon exposure to the desired analyte. In fact, this strategy has been successfully employed in biosensors, using antibodies<sup>12,13</sup> or nucleic acid aptamers<sup>14</sup> as the active interlayer for the indirect detection of proteins and other analytes. Regarding atomic ions, the first report in the literature described the use of gold nanoshells for the measurement of protons (pH) upon ionization/deionization of the carboxylic group of 4-mercaptopbenzoic acid (MBA) when exposed to solutions with different pH.<sup>15</sup> In fact, similar sensors based on MBA-capped nanoparticles had been widely used for internal pH monitoring in living cells.<sup>16,17</sup> Other reports were subsequently published, describing the use of different organic ligands for the indirect SERS determination of atomic cations, such as Zn(II) with (40-(N-piperazinyl)terpyridine-dithiocarbamate<sup>18</sup> or Hg(II) and Pb(II) with MBA.<sup>19</sup>

\* Address correspondence to ramon.alvarez@uvigo.es.

Received for review July 6, 2011 and accepted August 1, 2011.

Published online August 01, 2011  
10.1021/nn2025176

© 2011 American Chemical Society

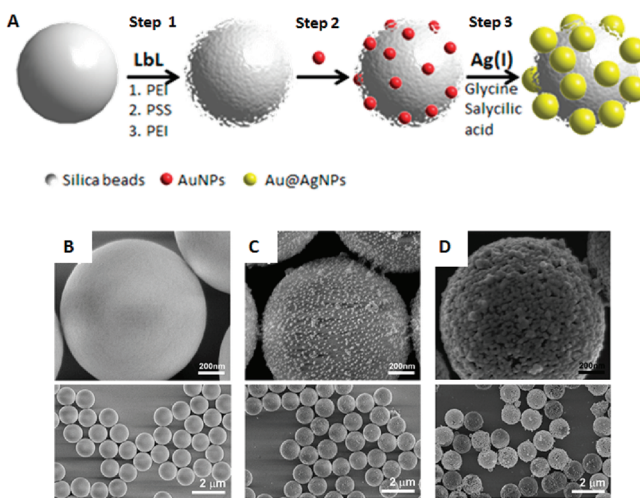


Figure 1. (A) Schematic drawing for the fabrication of micrometer-sized plasmonic hybrid materials. Scanning electron microscopy (SEM) images of the starting silica beads (B), after coating with gold nanoparticles (C), and after silver overgrowth on the gold nanoparticles (D).

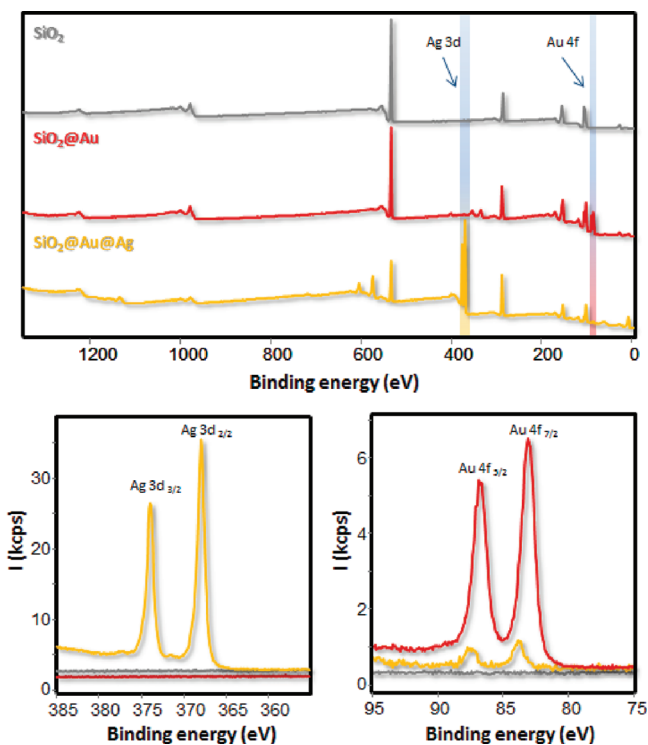
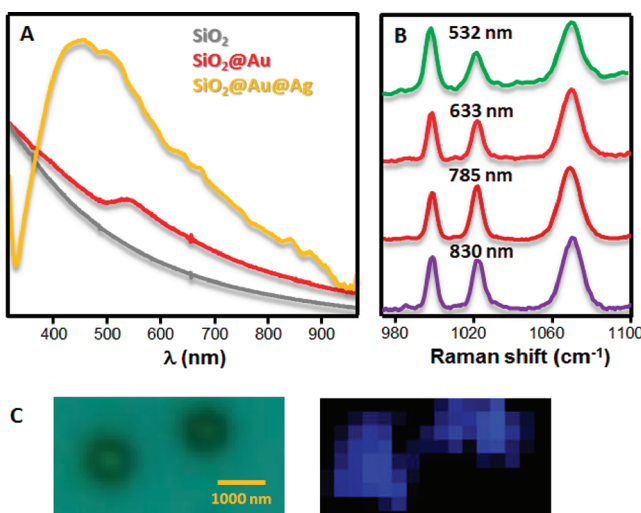


Figure 2. Survey and HR-XPS spectra of  $\text{SiO}_2$ ,  $\text{SiO}_2@\text{Au}$ , and  $\text{SiO}_2@\text{Au}@\text{Ag}$ .

One of the drawbacks of such an indirect SERS approach relies on the fact that rather nonpolar organic ligands need to be self-assembled on the metallic surfaces of colloidal nanoparticles. Colloidal stability can thus be reduced in the case of several ligands (e.g., hydrophobic ones), which in turn would promote aggregation. Most of the above-mentioned reports were demonstrated on nanostructured thin films, which are adequate for monitoring environmental processes but not for the fabrication of miniaturized sensors. A suitable alternative comprises the fabrication of

plasmonic surfaces on submicrometer or micromaterials used as supports, thus generating a stable platform containing a dense collection of hot spots.<sup>20</sup>

We demonstrate here the use of surface-enhanced Raman scattering (SERS) spectroscopy for the indirect, quantitative detection of atomic anions. We developed a sensor based on the vibrational changes induced by the interaction of chloride with a Cl-sensitive molecular probe that has a high SERS cross-section. A plasmonic platform consisting of silver-coated, micrometer-sized silica beads was developed, which can overcome



**Figure 3.** (A) UV–vis spectra of  $\text{SiO}_2$ ,  $\text{SiO}_2@\text{Au}$ , and  $\text{SiO}_2@\text{Au}@\text{Ag}$  beads. (B) SERS spectra of BT on  $\text{SiO}_2@\text{Au}@\text{Ag}$  upon excitation with different laser lines, from the green to the NIR. (C) White light and SERS (band at  $999 \text{ cm}^{-1}$ ) images of two single  $\text{SiO}_2@\text{Au}@\text{Ag}$  beads.

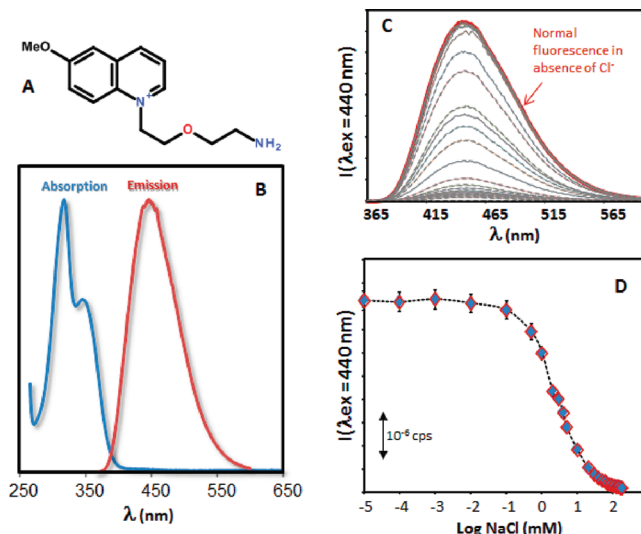


**Figure 4.** (A) Chemical structure of (amino-MQAE). (B) Electronic absorption and emission spectra of amino-MQAE. (C) Emission spectra of amino-MQAE as a function of chloride concentration. (D) Representative plot of the change of emission intensity vs  $\text{p}[Cl^-]$ .

undesired effects as colloidal aggregation upon self-assembly of the  $\text{Cl}^-$ -sensitive probe, while providing a dense collection of hot spots. Minute amounts of chloride down to the pM regime were quantitatively detected through the direct comparison of the SERS spectra of the ligand before and after interaction with chloride in aqueous solution.

## RESULTS AND DISCUSSION

The fabrication of the composite colloidal particles is schematically shown in Figure 1A. Briefly, the negatively charged surface of the selected support, in this case homogeneous silica beads with  $1 \mu\text{m}$  diameter (Figure 1B), was sequentially coated with polyelectrolytes of opposite charge, namely polyethylenimine

(PEI, positive), polystyrene sulfonate (PSS, negative), and again PEI, using the well-known layer-by-layer assembly protocol (step 1).<sup>21</sup> The outer PEI layer generates a highly positively charged surface that is appropriate for the adsorption of negatively charged gold nanoparticles (step 2, Figure 1C). Upon extensive cleaning to ensure that all nonadsorbed gold nanoparticles were removed, those which remained adsorbed were epitaxially overgrown with silver by the reduction of  $\text{Ag}^+$ , using salicylic acid in a glycine buffer (pH 9.5), at room temperature (step 3, Figure 1D). It is interesting to note that we found that gold seeds are preferred over silver for subsequent silver growth. This can be explained in terms of crystallography and chemical reactivity. While both metallic gold and silver

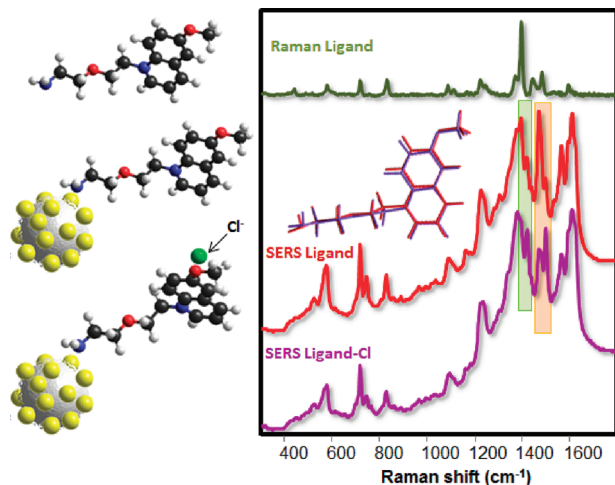


**Figure 5.** Left: Schematic representation of the detection process. Right: Raman and SERS spectra of amino-MQAE and SERS spectrum of amino-MQAE in the presence of an equimolar concentration of chloride ( $10^{-6}$  M). Optimized molecular geometry of amino-MQAE (at the M052X; 6-31+G\* theory level) in the presence (blue) and absence (red) of  $\text{Cl}^-$ . Samples were excited with a 532 nm laser line.

crystallize with the same crystallographic structure (face-centered cubic, fcc) and display very similar lattice parameters, the higher reactivity of silver, which tends to oxidize and form a thin oxide layer in water, makes the epitaxial growth difficult, resulting in extensive nucleation away from the adsorbed seeds.<sup>22</sup> The amount of added  $\text{Ag}^+$  was varied from 0.6 to 2.3  $\mu\text{mol}$  per mg of silica. Finally, an  $\text{Ag}^+$  concentration of 1.5  $\mu\text{mol}/(\text{mg of silica})$  was selected as optimal, since lower concentrations did not result in good interparticle plasmon coupling while higher concentrations yielded interconnected particles with the subsequent localized surface plasmon resonance (LSPR) radiative damping.<sup>23</sup> As a final product, this preparation process resulted in micrometer-sized hybrid plasmonic particles with a homogeneous coating of interacting silver particles<sup>24</sup> of around 50 nm in size (Figure 1D).

The bimetallic nature of the nanoparticles was demonstrated through X-ray photoelectron spectroscopy (XPS, Figure 2). As expected, the Ag 3d bands at 374.2 and 368.3 eV, characteristic of metallic silver, are only registered in the final  $\text{SiO}_2@\text{Au}@\text{Ag}$  sample, with 7.9 atom % in silver. However, the metallic gold characteristic 4f bands, at 88.0 and 84.3 eV, are clearly observed in the  $\text{SiO}_2@\text{Au}$  sample and their intensity was notably decreased (from 1.5 to 0.1 atom %) after silver growth, suggesting the nature of the particles as segregated (core–shell) nanoalloys rather than solid solutions.

UV-vis spectroscopy, carried out on colloidal dispersions of the particles in the three different stages (Figure 3A) showed that, whereas no LSPR band can be ascribed to the bare silica beads, a modest but clear band, centered at 535 nm, appears upon gold coating. This band notably increases in intensity and broadens due to the interparticle plasmon coupling,<sup>24</sup> while the maximum is blue-shifted after silver growth, which is consistent with the higher energy plasmon resonances

in silver nanoparticles. The optical enhancing properties of the materials were tested through SERS measurements, using benzenethiol (BT) as a model molecular probe.<sup>25</sup> Briefly, a small amount (10  $\mu\text{L}$ ) of diluted BT solution ( $10^{-4}$  M) was added per milliliter of  $\text{SiO}_2@\text{Au}@\text{Ag}$  colloidal dispersion. After waiting for thermodynamic equilibrium to be reached, the material comprising a self-assembled monolayer of BT was studied by SERS.<sup>26,27</sup> Contrary to nanostructured gold, which can be only excited with high wavelength laser radiation (from the red onward) due to strong damping when excited with green or more energetic lasers because of the characteristic gold interband transitions,<sup>28</sup> silver particles lead to strong SERS signals of the BT in a broad excitation window from the green (532 nm) to the NIR (830 nm) (Figure 3B). Notably and consistent with the literature, the SERS spectra are dominated by the vibrational modes of BT, corresponding to the ring breathings (999 and 1073  $\text{cm}^{-1}$ ), and the CH in-plane bending (1023  $\text{cm}^{-1}$ ), indicating a quasi-perpendicular orientation of its molecular plane with respect to the gold or silver surface.<sup>29,30</sup> Additionally, SERS mapping of single beads demonstrates that a single bead may be sufficient to obtain a high quality spectrum (Figure 3C).

As discussed in the introduction, the second key element of our sensing device comprises an ion-sensitive, in this case chloride sensitive, organic probe MQAE.<sup>31</sup> Here we used an amino-modified version of MQAE, 2-(2-(6-methoxyquinoliniumchloride)ethoxy)-ethanamine-hydrochloride (amino-MQAE), an organic fluorophore with a side chain containing a terminal amino group (Figure 4A), which is necessary for the covalent bonding of the molecule to the metallic surface. Amino-MQAE is characterized by an electronic absorption band with maxima centered at 315 and 341 nm. Upon excitation with the appropriate light (350 nm) amino-MQAE yields a strong emission band

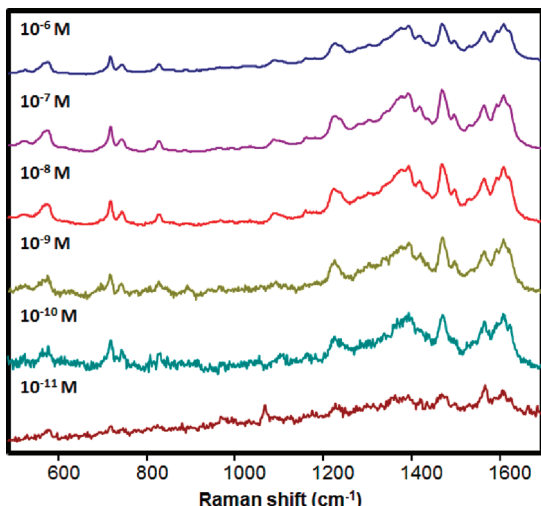


**Figure 6.** SERS spectra of amino-MQAE as a function of its own concentration in solution.

with a maximum located at 440 nm (Figure 4B). Notably, this fluorescence gets quenched in the presence of chloride ions. Figure 4C shows the decrease in the emission band as a function of the increase of chloride concentration in solution. This quenching effect has been exploited to investigate the  $\text{Cl}^-$  concentration near colloidal surfaces.<sup>32</sup> However, when the fluorescence quenching is plotted as a function of chloride concentration (Figure 4D), it is clear that the detection limit which can be achieved using this method is rather modest, around the micromolar regime.<sup>32</sup>

In this situation, SERS arises as a useful technique for the remote, ultrasensitive determination of  $\text{Cl}^-$ . Figure 5 shows the Raman and SERS spectra of amino-MQAE, as well as the SERS spectrum of amino-MQAE in the presence of an equimolar concentration of chloride. Considering the aromatic condensed rings as the molecular plane, the observed Raman bands correspond mainly to the in-plane vibrational modes, specifically ring stretchings (1483, 1444, and 1397  $\text{cm}^{-1}$ ), and bendings (1370 and 1232  $\text{cm}^{-1}$ ), while the out-of-plane modes carry a low vibrational Raman intensity, including CH waggings (830, 717  $\text{cm}^{-1}$ ), ring deformations (578  $\text{cm}^{-1}$ ), and ring waggings (438  $\text{cm}^{-1}$ ). Notably the band at 1086  $\text{cm}^{-1}$  can be ascribed to CO stretching.

As in the case of benzenethiol, samples for SERS were prepared by adding minute amounts ( $10 \mu\text{L}$ ) of the probe molecule at low concentrations ( $10^{-6} \text{ M}$  in this case) to the  $\text{SiO}_2@\text{Au}@\text{Ag}$  dispersion. Notably, Raman and SERS vibrational spectra were found to retain a close agreement, but specific changes were observed in the relative intensities between peaks. Changes in relative intensity are due to the surface selection rules<sup>33</sup> and can be used to discern the orientation of the molecule at the metallic surface.<sup>34</sup> First, with the use of the 532 nm laser line excitation at the red of the bulk plasma resonance, the main component of the field at the

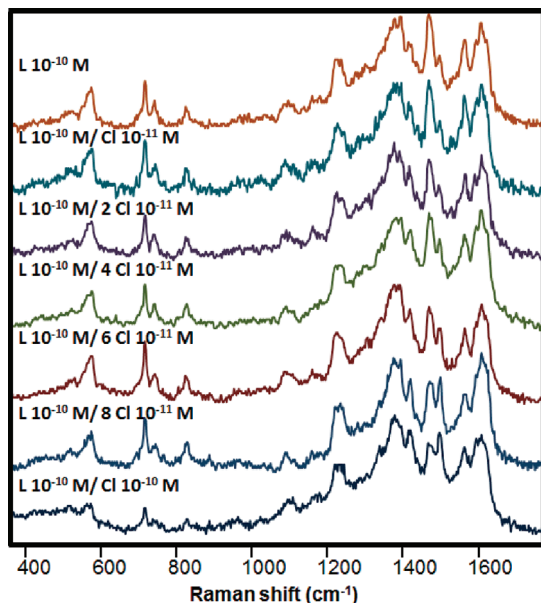


**Figure 7.** SERS spectra of amino-MQAE (ligand L)  $10^{-10} \text{ M}$  with increasing concentrations of chloride (from  $10^{-11}$  to  $10^{-10} \text{ M}$ ).

surface is the normal to the surface. Considering the high affinity of N-containing groups for silver,<sup>26,27</sup> the adsorbed molecule could be either flat on the metal surface, interacting by its N-heteroring, or with the molecular plane almost perpendicular to the metal surface if interacting through the terminal amino group. In keeping with the vibrational assignment, the observed SERS bands can be safely assigned to ring deformations in the plane of the molecule. In fact, the SERS spectra contain all of the in-plane vibrational frequencies (ring stretching and C—H bending in the 1000–1650  $\text{cm}^{-1}$  region) with remarkably strong relative intensity, as compared to those corresponding to out-of-plane modes. These latter observations discard the flat-on orientation and indicate that the ligand is bonded through the amino group with its aromatic chromophore perpendicular to the silver surface,<sup>35</sup> consistent with the higher reactivity toward silver or gold of the primary amines as compared with tertiary amines.<sup>26,27</sup> Similarly, the same results were obtained for amino-MQAE in the presence of chloride. Notwithstanding, consistent with density functional theory (DFT) calculations, the chloride atom interacts with the ring promoting a series of geometrical and electronic changes in the chromophore. Such changes can be clearly observed in the SERS spectra and are concentrated as well in the vibrational modes of the in-plane region of the spectra (from 1200  $\text{cm}^{-1}$  upward) and especially at those with a strong component of the C—N bond (1479 and 1497  $\text{cm}^{-1}$ ).

Taking all of this information into consideration, we studied the detection limits of the amino-MQAE dye (Figure 6). While the SERS spectrum of amino-MQAE (acquired upon excitation with the green line) can be fully recognizable at concentrations down to  $10^{-11} \text{ M}$ ,

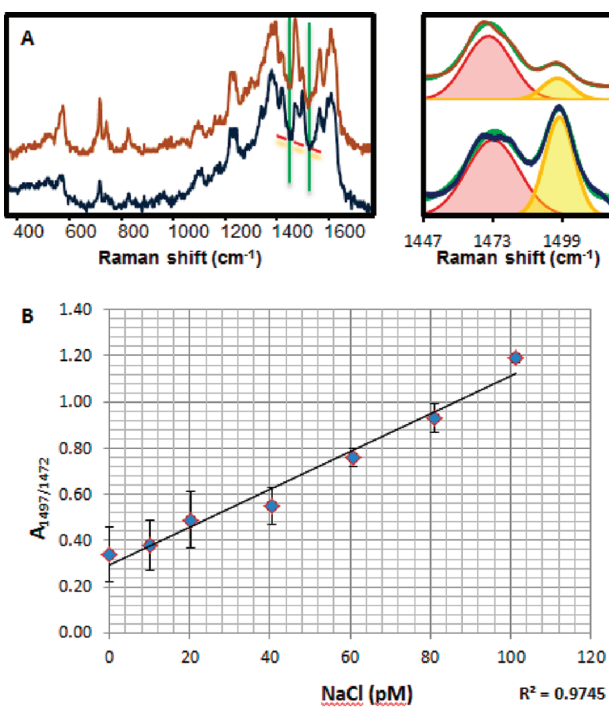


Figure 8. (A) SERS spectra of amino-MQAE ( $10^{-10}$  M) with and without chloride ( $10^{-10}$  M). Bands where the deconvolution was carried out are highlighted (brown and blue, experimental spectra; green, resulting spectra of coadding peak 1, red, and 2, yellow). (B) Linear plot of the  $1497$  and  $1472\text{ cm}^{-1}$  area ratio as a function of chloride concentration. Error bars represent the standard deviations within five replicated experiments.

the spectrum is still noisy and thus a concentration of  $10^{-10}$  M was selected for the quantitative identification of chloride.

Finally, the  $\text{SiO}_2@\text{Au}@\text{Ag}$  beads were capped with a submonolayer film of amino-MQAE and decreasing concentrations of  $\text{Cl}^-$  (from  $10^{-10}$  to  $10^{-12}$  M) were added. Figure 7 shows that the intensity of the *n*-related ring stretchings (at  $1479$  and  $1497\text{ cm}^{-1}$ ) decreases as the chloride concentration increases. In fact, this trend can be clearly observed with certainty down to concentrations of  $2 \times 10^{-11}$  M, which is equivalent to the picogram regime.

This indirect detection can also be exploited to obtain quantitative information regarding the concentration of chloride in the sample by simply comparing the ratio between the bands that change. To do so, the areas under the bands at  $1479$  and  $1497\text{ cm}^{-1}$  were deconvoluted assuming a Lorentzian shape, where the band position and the full widths at half maxima are fixed (Figure 8A).<sup>36</sup> Applying this process to all the spectra and plotting the band area ratio between  $1497$  and  $1479$  against concentration, the result is a linear correlation, with an impressive  $r^2$  value of  $0.9745$

(Figure 8B), which demonstrates the quantitative nature of this method of analysis.

## CONCLUSIONS

In summary, we have designed and fabricated a stable hybrid material comprising a micrometer-sized silica platform which is uniformly coated with nanostructured silver. This platform provides a remarkable SERS intensity due to the optimization of the plasmon coupling between silver nanoparticles, which results in a dense collection of hot spots. Furthermore, the vibrational response of a chloride sensitive dye was studied and exploited to devise a remote, indirect SERS sensor with the ability of selectively recognizing<sup>37</sup> and quantifying minute amounts of chloride, down to the picomolar regime. Since among the five halogens only three, chloride, bromide, and iodide, can readily be sensed by fluorescence quenching methods and only chloride is present in the cytosol of cells,<sup>38</sup> we anticipate this kind of sensor to be of key importance in the study of molecular and metabolic processes in living biological systems.

## EXPERIMENTAL MATERIALS AND METHODS

**Chemicals.** Silica microparticles, with  $1.16\text{ }\mu\text{m}$  diameter, were purchased from microParticles GmbH. All other chemicals were purchased from Aldrich and used without further purification. Water was purified using a Milli-Q system (Millipore).

**Silica Bead Functionalization and Synthesis and Adsorption of Gold Seeds ( $\text{SiO}_2@\text{Au}$ ).** Gold sols were prepared according to the standard sodium citrate reduction method,<sup>39</sup> by adding  $2\text{ mL}$  of  $1\text{ wt\%}$  sodium citrate solution to a  $100\text{ mL}$  boiling solution of  $\text{HAuCl}_4$  ( $5 \times 10^{-4}$  M) under stirring and additional boiling for

15 min. This method produces a deep-red dispersion of gold nanoparticles with an average diameter of around 15 nm.

Polyelectrolyte-coated  $\text{SiO}_2$  particles were prepared by adding 1 mL of polyethylenimine (PEI) ( $M_w = 25000$ , 1 mg mL<sup>-1</sup> in  $\text{NaNO}_3$  0.5 M) under weak sonication to 1 mL of the silica particles in water (1.6 g L<sup>-1</sup>). PEI adsorption was allowed for 1 h and then excess PEI was removed by three repeated centrifugation cycles (10 min, 3500 rpm). Polystyrene sulfonate (PSS) (MW = 1000000, 1 mg mL<sup>-1</sup> in  $\text{NaNO}_3$  0.5 M) was then deposited onto the PEI-coated silica particles under the same conditions, followed by deposition of an additional layer of PEI which forms the outermost layer.

Adsorption of the gold seeds was carried out by adding 5 mL of AuNPs colloid solution ( $5 \times 10^{-4}$  M) to 5 mL of functionalized  $\text{SiO}_2$  particles (1.16  $\mu\text{m}$ , 1.6 g L<sup>-1</sup>). The mixture was sonicated for 15 min. After 1 h the sample was washed by centrifugation (4  $\times$  3500 rpm, 30 min) to remove gold nanoparticles that did not adsorb on the silica surface and redispersed in 5 mL of water to obtain a final  $\text{SiO}_2@\text{Au}$  concentration of 1.6 g L<sup>-1</sup>.

**Silver Growth on the Gold Seeds ( $\text{SiO}_2@\text{Au}@\text{Ag}$ ).** Epitaxial growth of silver on the preformed gold seeds was carried out as follows:  $\text{SiO}_2@\text{Au}$  (1 mL, 1.6 g L<sup>-1</sup>) was added to 2.75 mL of glycine (0.4 M) buffer solution at pH 9.5. Then, 281.3  $\mu\text{L}$  of ascorbic acid 0.1 M and a variable concentration of  $\text{Ag}_2\text{SO}_4$  (15.2 mM) was added under weak sonication to reach final silver concentrations ranging from  $9.3 \times 10^{-4}$  to  $3.7 \times 10^{-3}$  M. After 30 min the reduction was finished and the sample was washed by centrifugation (4  $\times$  3500 rpm, 30 min) and redispersed in 1 mL of water to obtain a final concentration in particles of 1.6 g L<sup>-1</sup>.

**Synthesis of 2-(2-(6-Methoxyquinoliniumchloride)ethoxy)-ethanamine-hydrochloride (Amino-MQAE).** 2-Aminoethoxyethanol was protected at the amino function by reaction with phthalic anhydride in toluene under reflux overnight to yield the corresponding phthalimide. Subsequently, the alcohol group was brominated in a one-pot reaction by adding phosphorus tribromide under cooling at 0 °C. After being stirred at room temperature (RT), the mixture was poured into water, extracted with toluene, and recrystallized to yield 2-[2-(2'-bromoethoxy)ethyl]isoindoline-1,3-dione. The phthalimide-protected amino-MQAE was synthesized by heating 6-methoxyquinoline with 2-[2-(2'-bromoethoxy)ethyl] isoindoline-1,3-dione at 110 °C for 3 h. The alkylation product was recrystallized from acetone. Deprotection of the phthalimide was achieved by heating in hydrochloric acid overnight; the formed phthalic acid was separated by filtration. After recrystallization from methanol/aceton, the amino-MQAE was obtained as light yellow crystals.

**Characterization.** UV-vis-NIR spectra were recorded using an Agilent 8453 diode array spectrophotometer. XPS analysis of the samples was performed using a VG Escalab 250 iXL ESCA instrument (VG Scientific), equipped with aluminum K $\alpha$  1.2 monochromatic radiation at 1486.92 eV X-ray source. Binding energies (BEs) were referenced to the C1s on unspotted surfaces. The atomic concentrations were determined from the XPS peak areas using the Shirley background subtraction technique and the Scofield sensitivity factors. Transmission electron microscopy was carried out using a JEOL JEM 1010 microscope operating at an acceleration voltage of 100 kV. Scanning electron microscopy (SEM) images were obtained with a JEOL JSM 6700F field-emission microscope, using either lower secondary electron image (LEI) or secondary electron image (SEI) detectors.

**Theoretical Calculations.** Geometry optimizations at the DFT level were carried out with the Gaussian 09 (Revision A.02) suite of programs.<sup>40</sup> Computations with the Minnesota hybrid functional M052X by Zhao and Truhlar<sup>41</sup> ensure a high level of theory and an accurate estimation of the noncovalent interactions. The basis set used was a 6-31+G\* basis set. Geometrical convergence was obtained with at least a tight criterion. The terminal amino group of the amino-MQAE was fixed to represent the bond between the nitrogen atom and the metallic surface.

**Fluorescence and Surface-Enhanced Raman Scattering Spectroscopy.** Raman and SERS experiments were conducted in a micro-Renishaw InVia Reflex system. The spectrograph uses high resolution gratings (1800 or 1200 grooves cm<sup>-1</sup> for the visible or NIR, respectively) with additional band-pass filter optics, a

confocal microscope and a 2D-CCD camera. Excitation was carried out at different energies, using a laser line at 532 nm. Measurements were made using a macrosampler accessory.

The  $\text{SiO}_2@\text{Au}@\text{Ag}$ -amino-MQAE was desalting prior to fluorescence or SERS spectroscopy with a PD10 desalting column (Sigma, no. 54805) to remove eventual chloride contaminants. For the SERS characterization of the material, 10  $\mu\text{L}$  of benzenethiol (10<sup>-4</sup> M) were added to 1 mL aliquots (0.16 mg mL<sup>-1</sup>) of the  $\text{SiO}_2@\text{Au}@\text{Ag}$  suspension with different silver content to reach a final analyte concentration of 10<sup>-6</sup> M. Upon evaluation of the SERS intensity as a function of silver content, variable concentrations of amino-MQAE, from 10<sup>-3</sup> to 10<sup>-13</sup> M, were self-assembled onto the selected material, and its detection limits were determined by SERS. Subsequently, variable concentrations of chloride ions (from 10<sup>-10</sup> to 10<sup>-11</sup> M) were added to the  $\text{SiO}_2@\text{Au}@\text{Ag}$ -amino-MQAE sensor and studied by SERS using a 532 nm laser line. For quantitative analysis, bands were deconvoluted by Lorentzian shape, where the band position and the full widths at half maxima were fixed after applying a linear baseline (Figure 8A).<sup>36</sup>

Fluorescence spectra were recorded on a Fluorolog fluorescence spectrometer (Horiba) at sodium chloride concentrations from 0 to 140 mM in 10 mM steps. The sample stock solution was mixed with sodium chloride stock solutions (1:1) in a plastic reaction vessel before filling the mixture into a quartz cuvette. The fluorophor (amino-MQAE) was excited at 350 nm.

**Acknowledgment.** We thank C. Serra (CACTI, Universidade de Vigo) and J. M. Romo-Herrera for carrying out the XPS and SEM measurements, respectively. This work was funded by the Spanish Ministerio de Ciencia e Innovación (MAT2010-15374 and MAT2008-05755) the Xunta de Galicia (10 PXIB314218PR, 09TMT011314PR and 08TMT008314PR), the German Research Foundation (DFG, Grant PA794/11-1) and by the European Commission (Grant Nanognostics).

## REFERENCES AND NOTES

- Cavalli, S.; Polesello, S.; Valsecchi, S. Chloride Interference in the Determination of Bromate in Drinking Water by Reagent-free Ion Chromatography with Mass Spectrometry Detection. *J. Chromatogr. A* **2005**, *1085*, 42–46.
- Jackson, K. W.; Mahmood, T. M. Atomic Absorption, Atomic Emission, and Flame Emission Spectrometry. *Anal. Chem.* **1994**, *66*, 252R–279R.
- Mesaric, S.; Dahmen, E. A. M. F. Ion-Selective Carbon-Paste Electrodes for Halides and Silver(I) Ions. *Anal. Chim. Acta* **1973**, *64*, 431–438.
- Komaromy-Hiller, G.; Swallow, K. L.; Moulton, L. Inadequate Measurement of Urinary Chloride. *Ann. Clin. Lab.* **1998**, *28*, 347–53.
- Wegman, D.; Weiss, H.; Ammann, D.; Morf, W. E.; Pretsch, E.; Sugahara, K.; W., S. Anion-Selective Electrodes Based on Lipophilic Quaternary Ammonium Compounds. *Microchim. Acta* **1984**, *3*, 1–16.
- Kneipp, K. Surface-Enhanced Raman Scattering. *Phys. Today* **2007**, *60*, 40–46.
- Stiles, P. L.; Dieringer, J. A.; Shah, N. C.; Van Duyne, R. R. Surface-Enhanced Raman Spectroscopy. *Ann. Rev. Anal. Chem.* **2008**, *1*, 601–626.
- Moskovits, M. Spectroscopy: Expanding Versatility. *Nature* **2010**, *464*, 357.
- Sperling, R. A.; Rivera-Gil, P.; Zhang, F.; Zanella, M.; Parak, W. J. Biological Applications of Gold Nanoparticles. *Chem. Soc. Rev.* **2008**, *37*, 1896–1908.
- Alvarez-Puebla, R. A.; Liz-Marzán, L. M. SERS-Based Diagnosis and Biodetection. *Small* **2010**, *6*, 604–610.
- Vikesland, P. J.; Wigginton, K. R. Nanomaterial Enabled Biosensors for Pathogen Monitoring—A Review. *Environ. Sci. Technol.* **2010**, *44*, 3656–3669.
- Sanles-Sobrido, M.; Rodríguez-Lorenzo, L.; Lorenzo-Abalde, S.; González-Fernández, A.; Correa-Duarte, M. A.; Alvarez-Puebla, R. A.; Liz-Marzán, L. M. Label-free SERS Detection of Relevant Bioanalytes on Silver-Coated Carbon Nanotubes: The Case of Cocaine. *Nanoscale* **2009**, *1*, 153–158.

13. He, L. L.; Rodda, T.; Haynes, C. L.; Deschaines, T.; Strother, T.; Diez-Gonzalez, F.; Labuza, T. P. Detection of a Foreign Protein in Milk Using Surface-Enhanced Raman Spectroscopy Coupled with Antibody-Modified Silver Dendrites. *Anal. Chem.* **2011**, *83*, 1510–1513.
14. Kim, N. H.; Lee, S. J.; Moskovits, M. Aptamer-Mediated Surface-Enhanced Raman Spectroscopy Intensity Amplification. *Nano Lett.* **2010**, *10*, 4181–4185.
15. Bishnoi, S. W.; Rozell, C. J.; Levin, C. S.; Gheith, M. K.; Johnson, B. R.; Johnson, D. H.; Halas, N. J. All-Optical Nanoscale pH Meter. *Nano Lett.* **2006**, *6*, 1687–1692.
16. Kneipp, J.; Kneipp, H.; Wittig, B.; Kneipp, K. One- and Two-Photon Excited Optical pH Probing for Cells Using Surface-Enhanced Raman and Hyper-Raman Nanosensors. *Nano Lett.* **2007**, *7*, 2819–2823.
17. Pallaoro, A.; Braun, G. B.; Reich, N. O.; Moskovits, M. Mapping Local pH in Live Cells Using Encapsulated Fluorescent SERS Nanotags. *Small* **2010**, *6*, 618–622.
18. Zhao, Y.; Newton, J. N.; Liu, J.; Wei, A. Dithiocarbamate-Coated SERS Substrates: Sensitivity Gain by Partial Surface Passivation. *Langmuir* **2009**, *25*, 13833–13839.
19. Lee, S. J.; Moskovits, M. Visualizing Chromatographic Separation of Metal Ions on a Surface-Enhanced Raman Active Medium. *Nano Lett.* **2011**, *11*, 145–150.
20. Spuch-Calvar, M.; Rodriguez-Lorenzo, L.; Morales, M. P.; Alvarez-Puebla, R. A.; Liz-Marzan, L. M. Bifunctional Nanocomposites with Long-Term Stability as SERS Optical Accumulators for Ultrasensitive Analysis. *J. phys. Chem. C* **2009**, *113*, 3373–3377.
21. Decher, G. Fuzzy Nanoassemblies: Toward Layered Polymeric Multicomposites. *Science* **1997**, *277*, 1232–1237.
22. Rodriguez-Gonzalez, B.; Burrows, A.; Watanabe, M.; Kiely, C. J.; Liz Marzan, L. M. Multishell Bimetallic AuAg Nanoparticles: Synthesis, Structure and Optical Properties. *J. Mater. Chem.* **2005**, *15*, 1755–1759.
23. Schlegel, V. L.; Cotton, T. M. Silver-Island Films as Substrates for Enhanced Raman Scattering: Effect of Deposition Rate on Intensity. *Anal. Chem.* **1991**, *63*, 241–247.
24. Alvarez-Puebla, R.; Liz-Marzán, L. M.; García De Abajo, F. J. Light Concentration at the Nanometer Scale. *J. Phys. Chem. Lett.* **2010**, *1*, 2428–2434.
25. Alvarez-Puebla, R. A.; Dos Santos, D. S., Jr; Aroca, R. F. SERS Detection of Environmental Pollutants in Humic Acid–Gold Nanoparticle Composite Materials. *Analyst* **2007**, *132*, 1210–1214.
26. Ulman, A. Formation and Structure of Self-Assembled Monolayers. *Chem. Rev.* **1996**, *96*, 1533–1554.
27. Love, J. C.; Estroff, L. A.; Kriebel, J. K.; Nuzzo, R. G.; Whitesides, G. M. Self-Assembled Monolayers of Thiolates on Metals as a Form of Nanotechnology. *Chem. Rev.* **2005**, *105*, 1103–1170.
28. Zhao, J.; Pinchuk, A. O.; McMahon, J. M.; Li, S.; Ausman, L. K.; Atkinson, A. L.; Schatz, G. C. Methods for Describing the Electromagnetic Properties of Silver and Gold Nanoparticles. *Acc. Chem. Res.* **2008**, *41*, 1710–1720.
29. Carron, K. T.; Hurley, L. G. Axial and Azimuthal Angle Determination with Surface-Enhanced Raman Spectroscopy: Thiophenol on Copper, Silver, and Gold Metal Surfaces. *J. Phys. Chem.* **1991**, *95*, 9979–9984.
30. Saikin, S. K.; Chu, Y.; Rappoport, D.; Crozier, K. B.; Aspuru-Guzik, A. N. Separation of Electromagnetic and Chemical Contributions to Surface-Enhanced Raman Spectra on Nanoengineered Plasmonic Substrates. *J. Phys. Chem. Lett.* **2010**, *1*, 2740–2746.
31. Engblom, A. C.; Akerman, K. E. O. Determination of the Intracellular Free Chloride Concentration in Rat-Brain Synaptoneuroosomes Using a Chloride-Sensitive Fluorescent Indicator. *Biochim. Biophys. Acta* **1993**, *1153*, 262–266.
32. Riedinger, A.; Zhang, F.; Dommershausen, F.; Röcker, C.; Brandholt, S.; Nienhaus, G. U.; Koert, U.; Parak, W. J. Ratio-metric Optical Sensing of Chloride Ions with Organic Fluorophore–Gold Nanoparticle Hybrids: A Systematic Study of Design Parameters and Surface Charge Effects. *Small* **2010**, *6*, 2590–2597.
33. Moskovits, M.; Suh, J. S. Surface Selection-Rules for Surface-Enhanced Raman-Spectroscopy—Calculations and Application to the Surface-Enhanced Raman Spectrum of Phthalazine on Silver. *J. Phys. Chem.* **1984**, *88*, 5526–5530.
34. The orientation of molecules at metal surfaces can be inferred through the propensity toward enhancement of vibrational modes perpendicular to the surface. This propensity arises from the boundary condition which requires the electrostatic displacement,  $D$ , normal to the surface to be continuous across the interface:  $D_{\perp,\text{in}} = \epsilon_{\text{Ag}} E_{r=a}$ ;  $D_{\perp,\text{out}} = \epsilon_{\text{surroundings}} E_{r \neq a}$ . While the parallel component is simply:  $E_{||,\text{in} \neq a} = E_{||,\text{out} \neq a}$ . This leads to a preferential enhancement of the perpendicular electric field by a factor of  $\epsilon$ .
35. Aroca, R. F.; Clavijo, R. E.; Halls, M. D.; Schlegel, H. B. Surface-Enhanced Raman Spectra of Phthalimide. Interpretation of the SERS Spectra of the Surface Complex Formed on Silver Islands and Colloids. *J. Phys. Chem. A* **2000**, *104*, 9500–9505.
36. Thomas, G. J., Jr; Agard, D. A. Quantitative Analysis of Nucleic Acids, Proteins, and Viruses by Raman Band Deconvolution. *Biophys. J.* **1984**, *46*, 763–768.
37. Geddes, C. D. Optical Halide Sensing Using Fluorescence Quenching: Theory, Simulations and Applications—A Review. *Meas. Sci. Technol.* **2001**, *12*, R53.
38. Lodish, H. F. *Mol. Cell. Biol.*; Scientific American Books: New York, 1999.
39. Lee, P. C.; Meisel, D. Adsorption and Surface-Enhanced Raman of Dyes on Silver and Gold Sols. *J. Phys. Chem.* **1982**, *86*, 3391–3395.
40. Frisch, M. J.; Trucks, G. W.; Schlegel, H. B.; Scuseria, G. E.; Robb, M. A.; Cheeseman, J. R.; Scalmani, G.; Barone, V.; Mennucci, B.; Petersson, G. A. *et al.* *Gaussian 09*, revision A.02.; Gaussian, Inc.: Wallingford, CT, 2009.
41. Zhao, Y.; Truhlar, D. G. Density Functional for Spectroscopy: No Long-Range Self-Interaction Error, Good Performance for Rydberg and Charge-Transfer States, and Better Performance on Average than B3LYP for Ground States. *J. Phys. Chem. A* **2006**, *110*, 13126–13130.